THE JOURNAL OF PHYSICAL CHEMISTRY C

Article

pubs.acs.org/JPCC

Out-of-Equilibrium Assembly of Colloidal Particles at Air/Water Interface Tuned by Their Chemical Modification

Anna Kozina,*[,†] Salvador Ramos,[‡] Pedro Díaz-Leyva,[¶] and Rolando Castillo[‡]

[†]Instituto de Química, Universidad Nacional Autónoma de México, P.O. Box 70-213, 04510, Mexico City, Mexico

[‡]Instituto de Física, Universidad Nacional Autónoma de México, P.O. Box 20-364, 01000, Mexico City, Mexico

[¶]Departamento de Física, Universidad Autónoma Metropolitana Iztapalapa, San Rafael Atlixco 186, 09340 Mexico City, Mexico

Supporting Information

ABSTRACT: Assemblies of monolayers made of colloidal silica particles trapped at the air/water interface are prepared to have an increasing capillary interaction. Fine-tuning of the strength of interaction and its orientational specificity is achieved through isotropic or anisotropic colloid surface chemical modification or by adjusting the subphase surface tension. The capillary attraction between colloids is strong and specific enough to drive the particle organization out of equilibrium toward kinetically arrested assemblies. For isotropic particles, the square order competes with the hexagonal one at low area densities, which leads to their mutual frustration resulting in a polycrystalline solid at high densities. Anisotropic Janus particles attract so strongly and with such an orientational specificity that the resulting assemblies are the most dynamically arrested, although the crystal grains are highly ordered on the short length scale. We show that the particle anisotropic surface modification does not always result in a good long-range ordering at interfaces, although it opens up new possibilities of structure control.

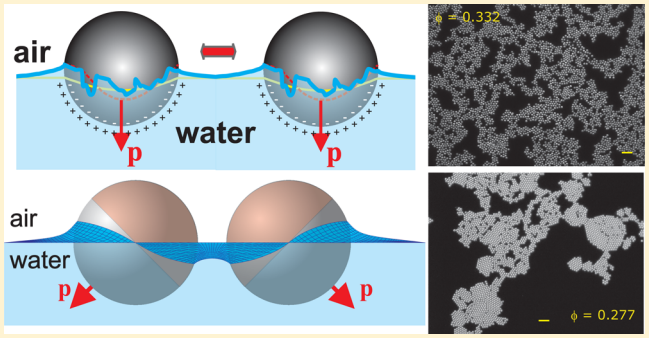

INTRODUCTION

The major effort in colloidal self-assembly is to gain control over the microscopic structure for desired modification of macroscopic properties to create novel functional materials (photonic, conductive, biological, etc.). One of the methods to obtain highly ordered structures in three dimensions (3D) implies layer by layer particle deposition assisted by interfaces.[1] Thus, the two-dimensional (2D) assembly becomes imperative as well as its experimental exploration. It remains a challenge to obtain highly ordered 2D structures because long-wavelength fluctuation modes in 2D are easily excited. Another obstacle is the geometrical mismatches (different particle sizes) that promote crystal defect propagation as grain boundaries.[2] Finally, excessively strong interparticle interactions may also impede the 2D ordering. Therefore, the assembly of colloids may be improved by precise control over their interactions. In equilibrium, the formation of a 2D solid from a liquid occurs in two steps via a hexatic phase.[3−10] In contrast, the assembly of spherical amphiphilic Janus colloids can result in a 2D orientational order that is driven by chemical patchiness. The broken rotational symmetry results in orientation-dependent interparticle interactions and even in arrested rotational dynamics.[11,12]

Self-assembly of a stable ordered structure occurs only when system parameters are tightly controlled, balancing two factors:[13] a thermodynamic impetus for components to form ordered structures and conditions that allow components to move randomly to arrange themselves into these structures. These factors tend to oppose each other. Conditions that are optimal from a thermodynamic viewpoint are often unsuitable for dynamic reasons and vice versa. The interactions between components must be strong enough to achieve an assembled structure that is lower in free energy than its dissembled parts to ensure the stability of the structure. Interactions should also be specific so that the desired structure is lower in free energy than other possible structures. Such specificity can be achieved through directional binding. These requirements of strength and specificity tend to inhibit the microscopic dynamics required for successful assembly. Thus, if interactions between components are too specific, typical encounters will not result in binding, and assembly will not happen on accessible time scales. Interactions should not be entirely specific, but nonspecific interactions lead to mistakes so that the random collisions of components will not always result in desired structure geometries. Therefore, intercomponent bonds must be weak enough so that thermal fluctuations can disrupt incorrect bonds, and components can dissociate and bind anew. They sample their local environment to select the most favorable modes of binding. This property of microscopic reversibility is a crucial method of error correction in self-

Received: June 17, 2016
Revised: July 8, 2016
Published: July 11, 2016

DOI: 10.1021/acs.jpcc.6b06145
J. Phys. Chem. C 2016, 120, 16879−16886

assembly. If the intercomponent binding is too strong, then this mechanism is suppressed, and the result is a kinetically trapped structure. These generic features determining self-assembly pathways are seen in a wide range of physical systems,[13,14] even though these systems may appear different with respect to their microscopic details. Here, we will present one example, the spherical isotropic colloids trapped at the air/water (a/w) interface. These are subjected to the attractive van der Waals and repulsive hard-core forces at short interparticle distances. Over the long range, they interact via a repulsive dipole−dipole interaction due to the ionization occurring in the submerged part of the particle. This repulsion is compensated by another long-range force acting on particles, namely, the attractive capillary force, which is rather specific because the particles must rotate in order to acquire the most energetically favorable positional and orientational configuration.[15−18]

In this work we present nonequilibrium self-assembly of spherical colloidal particles trapped at the a/w interface, and how the interplay between the dipole repulsion and capillary attraction can be tuned by surface isotropic or anisotropic chemical modification. Strength and specificity of particle interactions are modified and do not allow microscopic reversibility. Therefore, dynamical arrest interferes with the thermodynamic driving impetus leading to structural changes in the resulting particle organization. As we enhance capillary attraction by chemical modification of the whole particle surface, the resulting structures have a more frustrated hexagonal order, because of the amplification of the irregularities of the three-phase contact line, as more inhomogeneities on the particle surface are introduced. To go further, we break the interaction symmetry of the spherical particles by introduction of hydrophobic and hydrophilic hemispheres (Janus), which leads to a deeper dynamical arrest. Although the interaction between colloids and particularly between Janus particles trapped at interfaces have been reported,[19] they have usually been discussed only in terms of the interaction between a couple of particles. The consequences of their many-body interaction resulting from the noncentral capillarity on the order of the assemblies and the conditions to reach equilibrium or dynamical arrest have not been yet explored.

MATERIALS AND METHODS

Particle Surface Modification. *Isotropic Particles.* Dry silica particles with an average diameter of σ = 3.13 μm and polydispersity index 2.1% (Bang Laboratories, Inc., USA) and two types of surfaces were used. In the first case, bare silica particles (hydrophilic) were cleaned with piranha solution (30:70% v/v of 30% w/w water solution of hydrogen peroxide and 98% w/w of sulfuric acid), and then washed several times with deionized water (Milli-Q, resistivity ρ = 18.1 MΩ·cm) by sedimentation/redispersion method until pH is neutral. In the second case, the silica particle surface was modified with dichlorodimethylsilane (DCDMS) (Sigma-Aldrich, USA) by redispersing 20 mg of the bare silica particles in 0.1% v/v DCDMS/ethanol solution and stirring it overnight at room temperature. Next, these modified particles (hydrophobic) were washed three times with ethanol and several times with chloroform (both HPLC, Sigma-Aldrich, USA). The chloroform washing was repeated until the supernatant spread on the air/water interface reported no traces of undesired material when observed with Brewster angle microscopy (BAM). Finally, the particles were left to dry under vacuum.

Janus Particles. The synthesis of Janus particles followed the recipes from refs 20 and 21: 50 mg of the silica particles were cleaned as mentioned above for silanization and dispersed in 5 mL of the aqueous solution of didodecyldimethylammonium bromide (DDAB) with C = 0.011 g/L. This dispersion was added to 0.5 g of molten paraffin wax at 75 °C and stirred for 20 min with a magnetic stirring bar to form a stable wax-in-water emulsion. The DDAB concentration was chosen so that the particles were immersed at about a half of their volume. Then, the droplets were cooled to form solid colloidosomes, washed with deionized water to remove DDAB and unattached particles, and dried. The exposed particle surface was silanized with DCDMS in vapor according to ref 12 for 10 min, and then the wax was dissolved in chloroform and the particles were recovered.

Particle Monolayers. To perform the experiment at the air/water interface a Langmuir trough (KVS Nima, Biolin Scientific, Sweden) was used. The trough was isolated from vibrations and covered to avoid air currents from the surroundings. It was thoroughly cleaned with ethanol, chloroform, and MQ water prior to developing the monolayer. Before particle deposition, the Teflon barriers were completely closed, and the interface was observed with BAM (model 601, Nanofilm, Germany) to ensure that the water/air interface was surfactant free. To lower the surface tension of the subphase, an ethanol/water mixture (25:70 v/v) was used. Then, clean bare (hydrophilic) or modified (hydrophobic or Janus) particle were dispersed in chloroform/ethanol mixture and deposited on the water interface using a 2 mL glass syringe (Hamilton, USA). The surface with particles was also tested with BAM to be surfactant free. After particle deposition, a waiting time of about 20 min was used before the compression to allow solvent evaporation. An optical microscope (Axiotech vario 100 HD, Zeiss, Germany) provided with a 20× objective and a video camera (Pixelink, USA) were placed above the interface to record the images of the particles to be analyzed. This objective allowed us to detect about 8000 particles at high packing fractions to have better statistical analysis. To be as close to equilibrium as possible, the system was compressed slowly with area steps decreasing from 1 to 0.5 cm^2/step. The monolayer was left to equilibrate for each compression step: 30 min at low and 4 h at high packing fractions. The whole experiment lasts 4−5 days. A Wilhelmy plate was used to measure the lateral pressure $\Pi(A,T) = \gamma_0 - \gamma$, which is the surface pressure difference between the uncovered and the covered subphase, T is the temperature, and A is the area available to particles. The temperature was kept constant at 19 °C with the aid of a water circulating bath (Cole-Parmer 1268−24, USA) with a precision of ±0.1 °C. All the experiments were carried out in a clean-room laboratory to avoid contamination.

Data Analysis. *Radial Distribution Function (RDF).* The RDF $g(r)$ describes on average the probability of finding a particle at a distance r away from a given reference particle. Once the particle positions r_i are determined, $g(r)$ can be calculated as follows[22]

$$g(r) = \frac{1}{\rho^2}\left\langle \sum_i \sum_{j\neq i} \delta(r_i)\delta(r_j - r) \right\rangle \quad (1)$$

where $\rho = N/A$ is the average surface number density of particles. In the experiment, the averages are taken over N particles in the field of view of area A.

DOI: 10.1021/acs.jpcc.6b06145
J. Phys. Chem. C 2016, 120, 16879−16886

Bond Orientational Correlation Functions (BOCF) $g_6(r)$ and $g_4(r)$. The total bond orientational order parameter ψ_s can be calculated as an average of the individual bond orientational parameters $\varphi_{s,k}$:

$$\psi_s = \langle \varphi_{s,k} \rangle = \frac{1}{N}\left[\sum_{k=1}^{N} \varphi_{s,k}\right] = \frac{1}{N}\sum_{k=1}^{N}\frac{1}{n}\sum_{j=1}^{n} e^{is\theta_{kj}} \tag{2}$$

Here, the net sum is carried out over n nearest neighbors, θ_{kj} is the angle between an arbitrarily chosen axis and the bond joining neighbors k and j, N is the total number of analyzed particles. ψ_s evaluates on average the extent to which the bonds between the kth particle and its n neighbors present s-fold symmetry ($s = 6$ or 4). $\psi_s \sim 0$ in a liquid disordered phase, and $\psi_s \sim 1$ in a 2D lattice with perfect s-symmetry. The BOCF $g_s(r)$ is then defined as

$$g_s(r - r') = \frac{\langle \Psi_s^*(r)\Psi_s(r') \rangle}{\langle \rho(r)\rho(r') \rangle} \tag{3}$$

where

$$\Psi_s(r) = \sum_{k=1}^{N} \delta(r - r_k)\varphi_{s,k} \tag{4}$$

and

$$\rho(r) = \sum_{k=1}^{N} \delta(r - r_k) \tag{5}$$

The asterisk indicates complex conjugation.

Image Analysis. Recorded image sequences (16 fps) from the w/a interface with the microspheres were converted into 8-bit digitized images of 1392 × 1040 pixels, from which particle positions could be obtained using the method developed by Crocker and Grier,[23] which allows the location of particle centroids with an approximate precision of 1/5 pixel. Particle positional data enabled us to calculate the RDFs and the BOCFs given by eqs 1 and 3, respectively, using standard procedures.[24,25] For BOCF analysis, first, the nearest-neighbor detection was performed based on the RDF first peak position.

Correlation functions were obtained at several packing fractions, and to get useful statistics a significant number of frames was analyzed (1000−2000). To avoid artifacts reported in ref 26 due to optical detection, the interparticle distance was determined at close-packing conditions taking into account the real geometric particle diameter. It is important to note that at low packing fractions, the monolayer is sensitive to movement by tiny air currents in spite of the care taken to isolate the system. This is a constraint when a large number of optical images are acquired during extended periods of time. As a consequence, the correlation functions are noisier at low packing fractions. Besides, the dynamic structure factors $F(q,t)$ cannot be calculated from the correlation of the Fourier transformed images. For this reason, a particle tracking algorithm was applied that consisted of definition of the relative interparticle distances for different particle pairs. Then, the relative mean square displacements of the particles in the pairs could be calculated and autocorrelated in time.

Fractal Dimension. The fractal dimension d_f was calculated using the Minkowski-Bouligand algorithm, which is also known as "box counting" method. Here, d_f is estimated as an exponent of a power law:[27]

$$d_f = \lim_{L\to 0} \frac{\log N(L)}{\log \frac{1}{L}} \tag{6}$$

where $N(L)$ is the number of the boxes occupied by the object and L is the characteristic length of these boxes.

RESULTS AND DISCUSSION

For small particles, the deformation of the interface due to gravity is negligible (Bond number ≪1),[28] and the flotation level of particles is determined only by their contact angles. The mechanism of attraction is based on a nonuniform wetting of the particle caused by the irregular shape of the three-phase contact line.[15−18] The irregularity of the contact line comes from chemical inhomogeneities or local surface roughness resulting in the contact line pinning at small "defect" regions that cause the perturbation.[29−31] Since the interface surrounding the particles is distorted, the excess surface area and, consequently, the energy may be minimized when two adjacent particles assume an optimum relative orientation and distance. The most significant contribution to the surface deformation is a capillary quadrupolar term for the isotropic spherical particles that gives rise to an orientation-dependent interaction energy

$$\Psi = 12\pi\gamma H_2^{A} H_2^{B} \cos(2\varphi_A - 2\varphi_B)(r_c/r)^4 \qquad r \gg r_c \tag{7}$$

between two particles A and B (Figure 1a and b), which is much larger than the thermal energy k_BT (~10^5 k_BT). Here r_c is

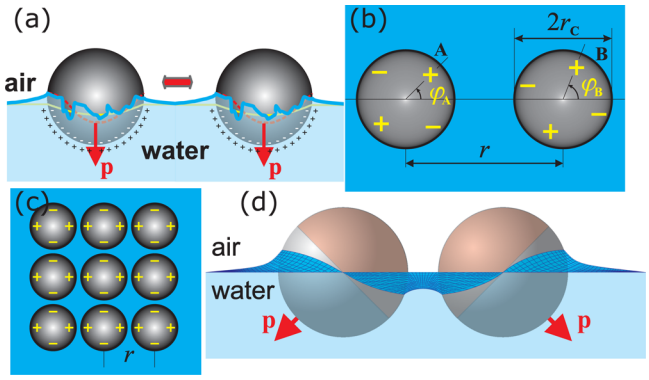

Figure 1. (a) Sketch of capillary attraction due to irregularities of the three-phase contact line (exaggerated for clarity). (b) Sketch of two capillary quadrupoles, A and B, separated by distance r and mutually orientated by angles φ_A and φ_B (view from above). The signs + and − mark convex and concave local deviations of the contact line from planarity. (c) Equilibrium lattice of capillary quadrupoles. (d) Spherical Janus particles in a nonequilibrium position interacting through a deformed interface.

the r coordinate at contact, φ_i is the subtended angle between the diagonals of the respective quadrupoles and the connecting line between particle centers, γ is the surface tension and H_2^i is the height of the meniscus at the contact line for i particle,[16,17,32] k_B is the Boltzmann constant and T is the absolute temperature. At short distances eq 7 is more complex.[17] Recent direct measurement of the interaction force between two particles at the oil/water interface is consistent with a capillary r^{-4} quadrupole interaction.[33]

Figure 2 confirms the presence of a long-range quadrupolar attraction for bare particles. We managed to capture the process of growth of a dense cluster through sequential images, where

DOI: 10.1021/acs.jpcc.6b06145
J. Phys. Chem. C 2016, 120, 16879−16886

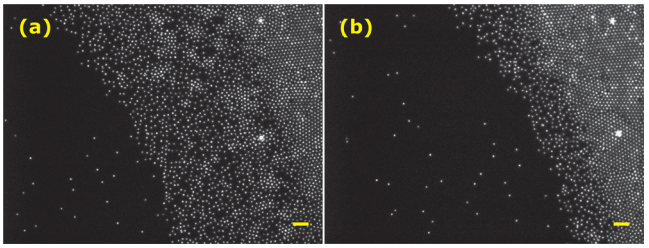

Figure 2. Dense cluster of bare particles at low ϕ growing at the a/w interface. Image time lag between (a) and (b) is 60 s; bars = 20 μm.

the long range of attraction is evident. In Figure 2a we observe an out-of-equilibrium dilute fluid (left), a dense fluid, and a growing solid-like cluster (right). Particles in Brownian motion attract each other especially in the intermediate region (movie in SI). Note that the large bright particles help to observe the evolution of the cluster. In Figure 2b grain boundaries in the cluster can already be observed.

To contrast the observations, two packing fraction regimes are described for isotropic particles: highly and loosely packed.

Isotropic Particles at High Packing Fractions. Optical microscopy images of bare and isotropically modified particle monolayers at large packing fractions ϕ are shown in Figure 3. The monolayer structure is deeply in a solid-like state where the particles touch each other. However, crystal structure correlation is far from decaying algebraically as described below. Although the packing fraction is quite large, a polycrystalline structure is observed due to many crystal defects. The bare particles are more ordered as observed in the Fourier transformed images (insets Figure 3), and they reach a higher maximum packing before being expelled from the interface due to further compression. Modified particles assemble in less ordered monolayers.

The RDFs presented in Figure 4a show the features of a solid assembly with a characteristic splitting of the second peak indicating a well-packed second neighboring shell. The peak splitting is reached at higher packing fractions for the monolayers of modified particles. However, the function envelopes indicate that all the functions decay with distance exponentially as $e^{-r/\zeta}$ and not algebraically as expected for a 2D solid in equilibrium. The positional order of the modified particles decays even faster than that of bare particles, as described by the correlation length ζ_m further revealing order frustration. The BOCFs $g_6(r)$ (Figure 4b) also decay exponentially for all the studied cases, except for bare particles at ϕ_b = 0.903, where it decays algebraically.

We suggest the following explanation. The effective potential that governs the structure must be the superposition of the orientation-dependent capillary (eq 7) and all the radial electrostatic contributions. If $H_2^A \sim H_2^B$, as in an array of colloidal particles similarly prepared, the capillary interaction implies that the particles will spontaneously move and rotate attempting to form a two-dimensional square lattice with a zero phase shift as illustrated in Figure 1c. The hexagonal order is not completely favorable unless one restricts the area available to the system bringing the particles so close together that the isotropic repulsive terms of electrostatic origin dominate. Therefore, both orientational orders compete. The quadrupolar interaction frustrates hexagonal arrays because the optimum relative orientations cannot be reached between all the particles at the same time. However, the orientation specificity of the capillary force is not very strong and, therefore, the hexagonal

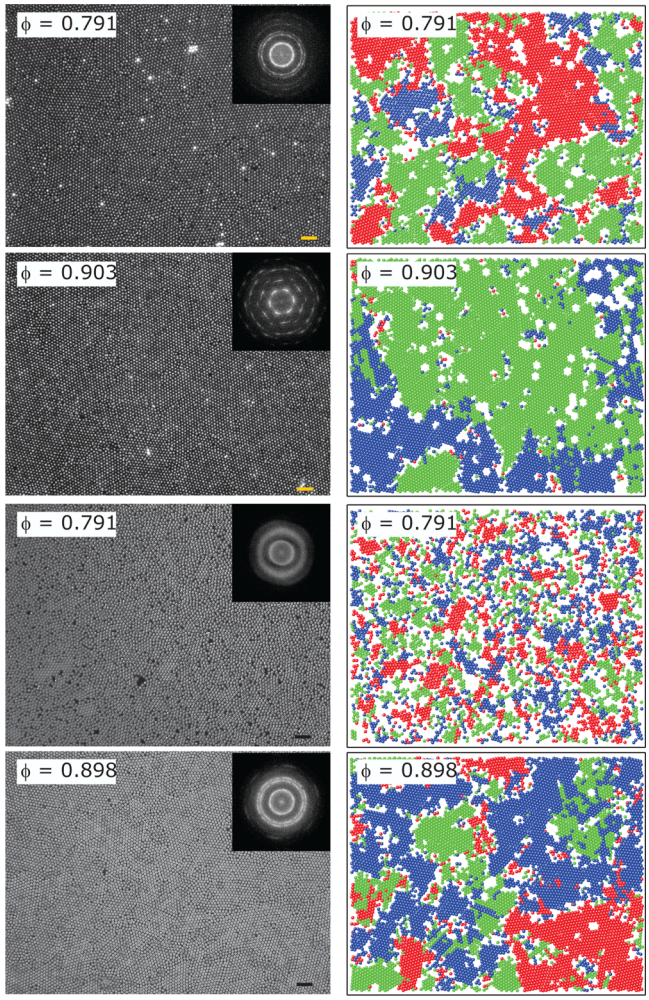

Figure 3. Left-hand column: optical micrographs of monolayers of bare (top two) and modified (bottom two) particles, bars = 20 μm. Insets: Corresponding Fourier transforms. Right-hand column: solid domains in the corresponding left-hand side micrographs colored according to the sixfold coordinated particle orientation with a threshold of 20° for corresponding ϕ's.

order prevails. Nevertheless, this subtle interaction (specificity) introduces anisotropy and also explains why $g_6(r)$ decays so fast as density slightly declines at high ϕ. The modified particles present more chemical surface defects due to nonhomogeneous coverage that promotes more definite irregularity of the three-phase contact line. Also, probably, the shape of the irregularities is different on different particles. On the other hand, since the particles are less submerged, the screening of the surface charge results in a weaker dipole repulsion. The stronger capillary attraction and the weaker dipole repulsion lead to a faster order correlation decay for modified particles as shown in Figure 4. Here, the orientational specificity of the capillary force is stronger than in the case of bare particles (H_2^i terms are larger).

Another aspect of the orientational order competition is the promotion of defects, i.e., as grain boundaries, as the capillary interaction increases. We observe marked differences in the monolayers depending on whether they were made of bare or modified silica. Figure 3 presents domains in silica monolayers at two different packing fractions. Along the whole field of view, we observe polycrystalline areas consisting of domains separated by grain boundaries. Each domain consists of particles with six neighbors. The crystal defects, particles with

DOI: 10.1021/acs.jpcc.6b06145
J. Phys. Chem. C 2016, 120, 16879−16886

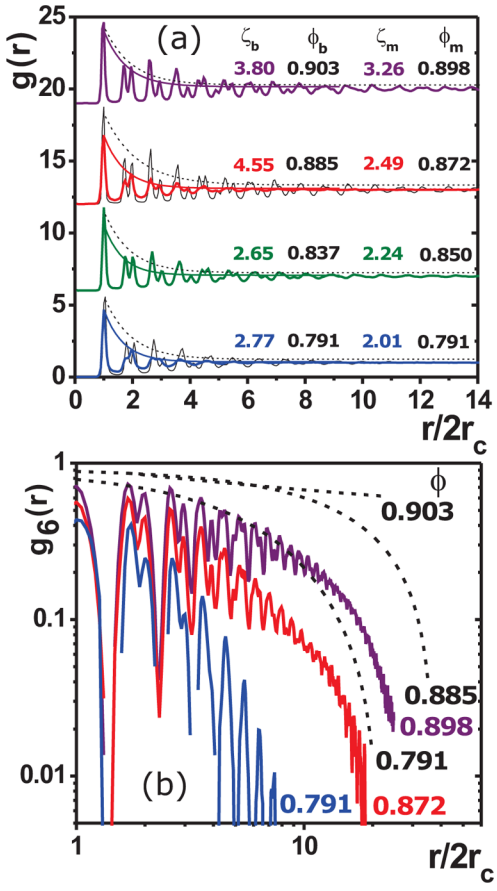

Figure 4. (a) RDFs for bare (two thin black solid lines) and modified (thick colored solid lines) particle monolayers with the corresponding exponential order decays (ζ_b and ζ_m) for the RDF envelopes (bare: black dashed lines, modified: thin colored solid lines), vertically shifted for clarity. (b) $g_6(r)$ for modified (colored thick lines) and correlation envelopes for bare (black dashed lines) particles. Numbers indicate the corresponding ϕ's.

nearest-neighbor numbers other than 6, are white voids. The grains that differ in orientation by more than 20° have different colors (right-hand column of Figure 3, a reference is chosen to be zero-angle oriented). The grain size grows as ϕ increases. The defects are expelled from crystal domains to the grain boundaries and can form their own network. The grains made of modified particles are smaller than those made of bare particles for similar packing fractions. Actually, at the packing of modified particles ϕ = 0.791, the grains are tiny inside the frozen disordered liquid, which looks analogous to crystal nucleation of hard-sphere systems with depletion attraction close to glass or gel transition.[34] A detailed analysis of grain boundaries is underway.

Isotropic Particles at Low Packing Fractions. At low ϕ, cluster formation reveals the anisotropy resulting from capillary attraction discussed above (Figure 5 and movies in SI). Here, strings and clusters with 2D square lattice order are noticeable. Both BOCFs $g_6(r)$ and $g_4(r)$ evaluated for images of Figure 5 are presented in Figure 6. They decay extremely fast indicating a very short-range order. Although the square order does not prevail, its contribution is not negligible. Since $g_6(r)$ is rather sensitive even to a small fraction of a nonhexagonal lattice (see SI), this contribution of the square order results in a significant crystallization frustration at high ϕ's. As mentioned above, for the modified particles the net capillary attraction is stronger

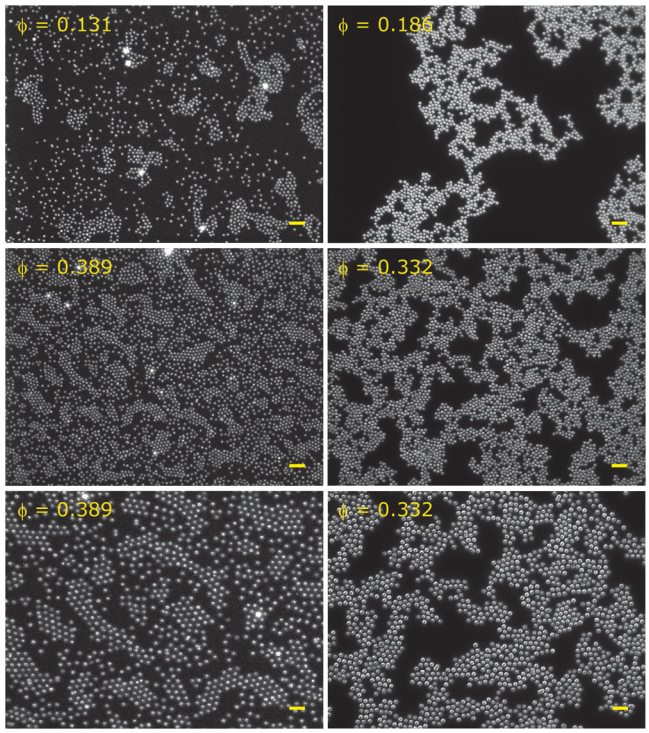

Figure 5. Optical micrographs of monolayers of bare (left) and modified (right) particles at low ϕ's. Two upper rows: bars = 20 μm and lower row: bars = 10 μm.

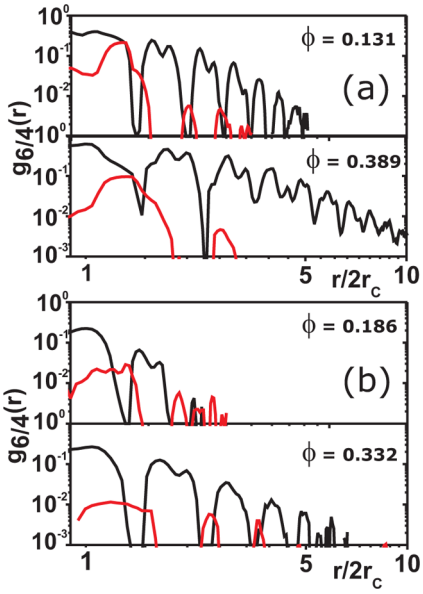

Figure 6. $g_6(r)$ (black) and $g_4(r)$ (red) at the corresponding ϕ's for (a) bare and (b) modified particles.

than for bare particles. In this case, the clusters are not prone to reshaping when they collide during compression. As far as they touch, they stick together forming a 2D long-lived spanning network extending along the field of view. There are no free particles. Particle dynamics are arrested in a similar way as in 3D colloidal suspensions with competing interactions.[35] Since the particles are not able to rearrange from the beginning at low ϕ's, the square lattice contribution is preserved at larger ϕ's and the hexagonal order frustration is stronger (Figure 3). In contrast, at low ϕ's the bare particles are more loosely packed,

DOI: 10.1021/acs.jpcc.6b06145
J. Phys. Chem. C 2016, 120, 16879−16886

they do not touch, and particle motion is well observed (see SI). This bare particle motion may lead to a conclusion that the system is close to equilibrium. Thus, in order to verify out-of-equilibrium behavior, we calculated time correlation functions for several particle pairs. Figure 7 shows some of these

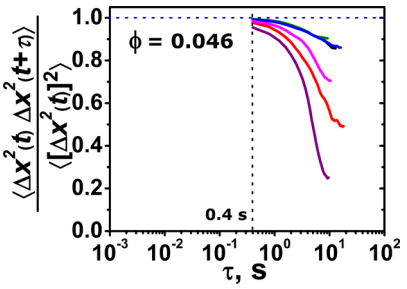

Figure 7. Typical examples of time autocorrelation of the mean square displacement for several pairs of bare particles at a given ϕ (corrected for convection). The time t = 0.4 s is the shortest sampling time accessible by the optical microscopy technique used.

functions. There is a distribution of time decay, and some of the correlation functions do not decay to zero indicating frozen dynamics. The distribution of decay times is a feature of a rather heterogeneous dynamics typical for dynamically arrested systems. This allows us to conclude that even at very low packing fractions of bare particles the system is out of equilibrium.

How can the capillary attraction be tuned besides the superficial particle functionalization? The answer is in eq 7: by variation of the subphase surface tension. Indeed, Figure 8

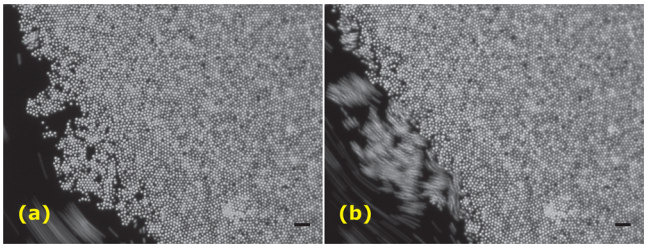

Figure 8. Hexagonal order domains of modified particles at the a/ew interface. The particles are easily separated by subtle subphase flow. No long-range attraction is observed (bars = 20 μm).

presents modified particles at the air/(ethanol+water) (a/ew) interface. In this case, the capillary and dipole interactions are substantially reduced due to a lower γ of the mixture ($\gamma_w \approx 72$ mN/m vs $\gamma_{ethanol} \approx 22$ mN/m) and a lower colloidal ionization. The attraction is clearly of a short range but it is so weak that a subtle subphase flow can easily separate the particles (see SI). The hexagonal order is more evident here than in the case of pure water as a subphase.

Janus Particles. Janus amphiphilic spheres under non-equilibrium conditions rotate away from the energetically favorable upright orientation (Figure 1d), where the capillary quadrupole term is the lowest allowed multipole order.[36] The larger the amphiphilicity of the particle surface, the more tilted the particle orientation is and the greater the interface deformation. Now, the lowest multipole order, the dipolar capillary interaction term, becomes dominant, and the in-plane repulsive dipole−dipole interaction due to the ionization is reduced because the dipole is also tilted. Two neighboring Janus spheres are expected to realign to achieve the state of minimum energy. Regions with an equal sign overlap and form a capillary bridge. Numerical calculations have shown[36] that the potential for small spacing between Janus spheres is $V/(\gamma r_c) = A \times (r_c/r)^3$. Here A is a function of amphiphilicity, tilting, and relative in-plane alignment of the particles. At the optimum alignment this coefficient increases with an increase of particle amphiphilicity indicating stronger interactions due to larger interface distortions. The result of the introduction of the surface anisotropy of Janus type is observed in Figure 9. Janus

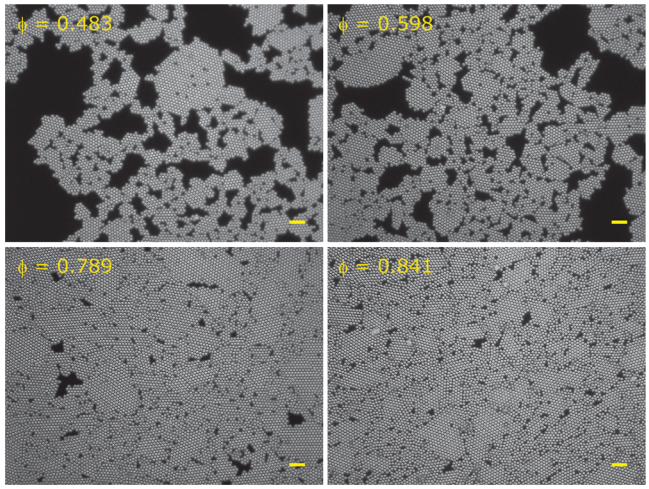

Figure 9. Janus particles. Optical micrographs at the corresponding ϕ's (bars = 20 μm).

spheres form hexagonally organized domains that are interconnected along the whole field of view. Again, no free particles are observed. The positional order decays exponentially with distance (Figure 10). The correlation length ζ_j is

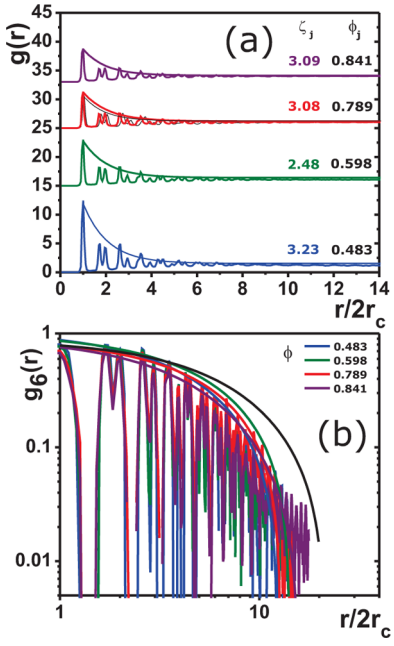

Figure 10. Janus particles. (a) $g(r)$ and (b) $g_6(r)$ with the corresponding exponential order decays (ζ_j for the $g(r)$ envelopes) vertically shifted for clarity. In both figures black line corresponds to the monolayer of bare particles at ϕ = 0.791.

DOI: 10.1021/acs.jpcc.6b06145
J. Phys. Chem. C 2016, 120, 16879−16886

larger as compared to that for isotropic particles at similar ϕ indicating a slower order correlation loss. Surprisingly, the short-range positional order (up to four particle diameters) is more pronounced at lower ϕ's than at high ϕ's as observed from $g(r)$ peak heights. The favorable order for Janus particles is hexagonal because of capillary dipole orientation.[36] However, the larger strength and orientational specificity of attraction as compared to the isotropic particles quenches the system to a deeper kinetically arrested state. Thus, the particles inside the clusters cannot easily rearrange. On reduction of the available area during the monolayer compression, the clusters are not prone to fill the voids as they collide. Therefore, the particles located at the cluster edges are forced to lose their hexagonal symmetry. In this case, the short-range hexagonal order is frustrated at larger ϕ's and the system cannot reach the same large packing densities as the one made of isotropic bare particles before the monolayer collapses. Intercluster packing is hindered as can be observed from the fractal dimension (Table 1) as compared to the isotropic spheres. Even lowering of the subphase γ does not cause the particles separation (see SI). The interaction between Janus particles is really strong when they are trapped at interfaces.

Table 1. Fractal Dimensions

ϕ	d_{bare}	ϕ	$d_{modified}$	ϕ	d_{janus}
0.131	1.96	0.332	1.94	0.277	1.63
0.159	1.94	0.372	1.94	0.457	1.80
0.317	1.98	0.569	1.98	0.598	1.87
0.389	1.98	-	-	-	-

CONCLUSIONS

We have discussed how the requirements of strength and specificity tend to inhibit the microscopic dynamics required for successful long-range ordered assembly in colloids trapped at interfaces. These generic features of self-assembly can be observed in many physical systems, although they may be made of different microscopic constituents. An example could be the self-assembly of DNA-coated colloids with complementary DNA strands.[37] Specific interactions are not adequate for long-range ordering if the intercomponent bonds are not weak enough that incorrect bonds can be disrupted by thermal fluctuations. This property of microscopic reversibility is a crucial method of error correction in self-assembly.

We have shown that tuning the strength and specificity of the interactions between particles trapped at interfaces gives rise to a new method of realization of assemblies with a variety of different structures. The microscopic dynamics required to reach equilibrium structures are more arrested going from bare particles to the ones with more complex surface modification, due to capillary attraction. The interactions can also be modified by varying the subphase surface tension. Our results show that more sophisticated particle surface modification will not necessarily result in a better long-range ordering, although it opens up new possibilities of structure control. The results appeal for molecular simulations with orientation dependent interactions and put questions toward the different possible orderings and effective interactions in anisotropic particles trapped at interfaces.

ASSOCIATED CONTENT

Supporting Information

The Supporting Information is available free of charge on the ACS Publications website at DOI: 10.1021/acs.jpcc.6b06145.

Phase separation events in a monolayer of bare particles between a low-density fluid phase and a condensed phase that is growing (ZIP)

Monolayer of bare particles at low packing fractions (ZIP)

Monolayer of modified particles at low packing fractions (ZIP)

Monolayer of modified particles at low packing fractions (ZIP)

Monolayer of modified particles trapped at the air/ethanol+water interface (ZIP)

Monolayer of Janus particles trapped at the air/ethanol +water interface (ZIP)

Details on data analysis and theoretical background (PDF)

AUTHOR INFORMATION

Corresponding Author

*E-mail: akozina@unam.mx. Phone: +525556224437.

Notes

The authors declare no competing financial interest.

ACKNOWLEDGMENTS

Financial support from SEP-CONACyT (177679 and 238618), CONACyT FC 77, DGAPA-UNAM (IN 110414 and IA 100215), and CONACyT Mexican Soft Matter Network are gratefully acknowledged.

REFERENCES

(1) Xia, Y.; Gates, B.; Yin, Y.; Lu, Y. Monodispersed Colloidal Spheres: Old Materials with New Applications. *Adv. Mater.* **2000**, *12*, 693−713.

(2) Gray, A. T.; Mould, E.; Royall, C. P.; Williams, I. Structural Characterisation of Polycrystalline Colloidal Monolayers in the Presence of Aspherical Impurities. *J. Phys.: Condens. Matter* **2015**, *27*, 194108−194119.

(3) Strandburg, K. J. Two-dimensional melting. *Rev. Mod. Phys.* **1988**, *60*, 161−207.

(4) von Grünberg, H. H.; Keim, P.; Maret, G. Phase Transitions in Two-Dimensional Colloidal Systems in *Soft Matter*, Gompper, G.; Schick, M., Eds.; Wiley & Sons, 2007.

(5) Bernard, E. P.; Krauth, W. Two-Step Melting in Two Dimensions: First-Order Liquid-Hexatic Transition. *Phys. Rev. Lett.* **2011**, *107*, 155704.

(6) Engel, M.; Anderson, J. A.; Glotzer, S. C.; Isobe, M.; Bernard, E. P.; Krauth, W. Hard-Disk Equation of State: First-Order Liquid-Hexatic Transition in Two Dimensions with Three Simulation Methods. *Phys. Rev. E* **2013**, *87*, 042134.

(7) Qi, W.; Gantapara, A. P.; Dijkstra, M. Two-Stage Melting Induced by Dislocations and Grain Boundaries in Monolayers of Hard Spheres. *Soft Matter* **2014**, *10*, 5449−5457.

(8) Kapfer, S. C.; Krauth, W. Two-Dimensional Melting: From Liquid-Hexatic Coexistence to Continuous Transitions. *Phys. Rev. Lett.* **2015**, *114*, 357028.

(9) Armstrong, A. J.; Mockler, R. C.; O'Sullivan, W. J. Isothermal-Expansion Melting of Two-Dimensional Colloidal Monolayers on the Surface of Water. *J. Phys.: Condens. Matter* **1989**, *1*, 1707−1730.

(10) Marcus, A. H.; Rice, S. A. Phase Transitions in a Confined Quasi-Two-Dimensional Colloid Suspension. *Phys. Rev. E: Stat. Phys., Plasmas, Fluids, Relat. Interdiscip. Top.* **1997**, *55*, 637−656.

DOI: 10.1021/acs.jpcc.6b06145
J. Phys. Chem. C 2016, 120, 16879−16886

(11) Shin, H.; Schweizer, K. S. Theory of Two-Dimensional Self-Assembly of Janus Colloids: Crystallization and Orientational Ordering. *Soft Matter* **2014**, *10*, 262−274.
(12) Jiang, S.; Yan, J.; Whitmer, J. K.; Anthony, S. M.; Luijten, E.; Granick, S. Orientationally Glassy Crystals of Janus Spheres. *Phys. Rev. Lett.* **2014**, *112*, 218301.
(13) Whitelam, S.; Jack, R. L. The Statistical Mechanics of Dynamic Pathways to Self-Assembly. *Annu. Rev. Phys. Chem.* **2015**, *66*, 143−163.
(14) Grant, J.; Jack, R. L.; Whitelam, S. Analyzing Mechanisms and Microscopic Reversibility of Self-Assembly. *J. Chem. Phys.* **2011**, *135*, 214505.
(15) Danov, K. D.; Kralchevsky, P. A.; Naydenov, B. N.; Brenn, G. Interactions between Particles with an Undulated Contact Line at a Fluid Interface: Capillary Multipoles of Arbitrary Order. *J. Colloid Interface Sci.* **2005**, *287*, 121−134.
(16) Stamou, D.; Duschl, C.; Johannsmann, D. Long-Range Attraction between Colloidal Spheres at the Air-Water Interface: The Consequence of an Irregular Meniscus. *Phys. Rev. E: Stat. Phys., Plasmas, Fluids, Relat. Interdiscip. Top.* **2000**, *62*, 5263−5272.
(17) Kralchevsky, P. A.; Denkov, N. D.; Danov, K. D. Interface: Interaction between Capillary Quadrupoles and Rheology of Particulate Monolayers. *Langmuir* **2001**, *17*, 7694−7705.
(18) Kralchevsky, P. A.; Denkov, N. D. Capillary Forces and Structuring in Layers of Colloid Particles. *Curr. Opin. Colloid Interface Sci.* **2001**, *6*, 383−401.
(19) Kumar, A.; Park, B. J.; Tu, F.; Lee, D. Amphiphilic Janus Particles at Fluid Interfaces. *Soft Matter* **2013**, *9*, 6604−6617.
(20) Jiang, S.; Schultz, M. J.; Chen, Q.; Moore, J. S.; Granick, S. Solvent-Free Synthesis of Janus Colloidal Particles. *Langmuir* **2008**, *24*, 10073−0077.
(21) Mugica, L. C.; Rodríguez-Molina, B.; Ramos, S.; Kozina, A. Surface Functionalization of Silica Particles for Their Efficient Fluorescence and Stereo Selective Modification. *Colloids Surf., A* **2016**, *500*, 79−87.
(22) Hansen, J. P.; McDonald, I. R. *Theory of Simple Liquids*; Academic: New York, 1986.
(23) Crocker, J. C.; Grier, D. G. Methods of Digital Video Microscopy for Colloidal Studies. *J. Colloid Interface Sci.* **1996**, *179*, 298−310.
(24) Allen, M. P.; Tildesley, D. J. *Computer Simulation of Liquids*; Clarendon Press: Oxford, 1987.
(25) Bonales, L. J.; Rubio, J. E. F.; Ritacco, H.; Vega, C.; Rubio, R. G.; Ortega, F. Freezing Transition and Interaction Potential in Monolayers of Microparticles at Fluid Interfaces. *Langmuir* **2011**, *27*, 3391−3400.
(26) Ramírez-Saito, A.; Bechinger, C.; Arauz-Lara, J. L. Optical Microscopy Measurement of Pair Correlation Functions. *Phys. Rev. E* **2006**, *74*, 030401.
(27) Falconer, K. *Fractal Geometry: Mathematical Foundations and Applications*; John Wiley: Chichester, 1990.
(28) Vella, D.; Mahadevan, L. The 'Cheerios effect'. *Am. J. Phys.* **2005**, *73*, 817−825.
(29) Joanny, J. F.; de Gennes, P. G. A Model for Contact Angle Hysteresis. *J. Chem. Phys.* **1984**, *81*, 552−562.
(30) Decker, E. L.; Garoff, S. Contact Line Structure and Dynamics on Surfaces with Contact Angle Hysteresis. *Langmuir* **1997**, *13*, 6321−6332.
(31) Sharifi-Mood, N.; Liu, I. B.; Stebe, K. J. Curvature Capillary Migration of Microspheres. *Soft Matter* **2015**, *11*, 6768−6779.
(32) Fournier, J.-B.; Galatola, P. Anisotropic Capillary Interactions and Jamming of Colloidal Particles Trapped at a Liquid-Fluid Interface. *Phys. Rev. E: Stat. Phys., Plasmas, Fluids, Relat. Interdiscip. Top.* **2002**, *65*, 031601.
(33) Park, B. J.; Furst, E. M. Attractive Interactions between Colloids at the Oil-Water Interface. *Soft Matter* **2011**, *7*, 7676−7682.
(34) Kozina, A.; Díaz-Leyva, P.; Palberg, T.; Bartsch, E. Crystallization Kinetics of Colloidal Binary Mixtures with Depletion Attraction. *Soft Matter* **2014**, *10*, 9523−9533.
(35) Zhang, T. H.; Klok, J.; Tromp, R. H.; Groenewold, J.; Kegel, W. K. Non-Equilibrium Cluster States in Colloids with Competing Interactions. *Soft Matter* **2012**, *8*, 667−672.
(36) Rezvantalaba, H.; Shojaei-Zadeh, S. Capillary Interactions between Spherical Janus Particles at Liquid-Fluid Interfaces. *Soft Matter* **2013**, *9*, 3640−3650.
(37) Wang, Y.; Wang, Y.; Zheng, X.; Ducrot, E.; Yodh, J. S.; Weck, M.; Pine, D. J. Crystallization of DNA-Coated Colloids. *Nat. Commun.* **2015**, *6*, 7253.

DOI: 10.1021/acs.jpcc.6b06145
J. Phys. Chem. C 2016, 120, 16879−16886